Journal of Applied Fluid Mechanics, Vol. 9, No. 4, pp. 1915-1925, 2016.
Available online at www.jafmonline.net, ISSN 1735-3572, EISSN 1735-3645.
DOI: 10.18869/acadpub.jafm.68.235.24820

3-D Numerical Study of Hydromagnetic Double Diffusive Natural Convection and Entropy Generation in Cubic Cavity

C. Maatki[1], W. Hassen[1], L. Kolsi[2,1†], N. AlShammari[2] M. Naceur Borjini[1] and H. B. Aissia[1]

[2]College of Engineering, Mechanical Engineering Department, Haïl University, Haïl City , Saudi Arabia
[1] Unité de Métrologie et des Systèmes Energétiques, Ecole Nationale d'Ingénieurs, 5000 Monastir, University of Monastir, Tunisia

†Corresponding Author Email: lioua_enim@yahoo.fr

(Received March 24, 2015; accepted September 8, 2015)

ABSTRACT

In the present work, the effect of magnetic field on double diffusive natural convection in a cubic cavity filled with a binary mixture is numerically studied using the finite volume method. Two vertical walls are maintained at different temperatures and concentrations. The study is focused on the determination of the entropy generation due to heat and mass transfer, fluid friction and magnetic effect. The influence of the magnetic field on the three-dimensional flow, temperature and concentration fields, entropy generation and heat and mass transfer are revealed. The main important result of this study is that the increase of Hartmann number damped the flow and homogenized the entropy generation distribution in the entire cavity.

Keywords: Entropy generation; Magneto convection; Heat and mass transfer.

NOMENCLATURE

$\vec{B}$	magnetic field
C	dimensionless species concentration
C'_h	high species concentration
C'_l	low species concentration
D	species diffusivity
$\vec{e}_X$	direction of magnetic field
g	acceleration of gravity
Ha	Hartmann number
$\vec{J}$	dimensionless current density
J	current density intensity
k	thermal conductivity
L	cavity side
Le	Lewis number
N	buoyancy ratio
$\vec{n}$	unit vector normal to the control volume surface
Nu	Nusselt number
Pr	Prandtl number
R	gas constant
Ra	Rayleigh number
S'_{gen}	generated entropy
Sh	Sherwood number
T	dimensionless temperature
t	dimensionless time
T'_c	cold wall temperature
T'_h	hot wall temperature
$\vec{u}$	dimensionless velocity
x, y, z	Cartesian coordinates
α	thermal diffusivity
β_T	coefficient of thermal expansion
β_C	coefficient of compositional expansion
Φ	dimensionless electric potential
φ_i	Irreversibility coefficient
μ	dynamic viscosity
ν	kinematic viscosity
ρ	density
σ_e	electrical conductivity
$\vec{\omega}$	dimensionless vorticity
$\vec{\psi}$	dimensionless stream function

Superscripts

'	dimensional variable

Subscripts

1,2,3,4	index of the Irreversibility coefficient
Max	maximum

1. INTRODUCTION

The natural convection which is produced by volume forces resulting simultaneously from temperature and concentration gradients is generally referred either to the thermosolutale convection or double diffusion. Beghein *et al*. (1992) studied numerically a steady-state thermosolutal convection in a square cavity filled with air, submitted to horizontal temperature and concentration gradients. The study in a two-fluid mixture in rectangular enclosure has drawn a great deal of research (Trevisan 1992 and Costa 1997). The double diffusive natural convection carried out in a two dimensional cavity filled with a binary fluid and subjected to horizontal temperature and concentration gradients with cooperating volume forces has been studied by Gobin and Bennacer (1996). They have shown that for a high Lewis number, the thermal transfer decrease as the buoyancy ratio increase.

The analytical and numerical study of double-diffusive natural convection in a rectangular enclosure filled with non-Newtonian fluid is carried out by Makayssi *et al*. (2008). Indeed, the authors proposed an analytical solution based on the approximation of parallel flow in the case of a shallow cavity. This analytical solution has good agreement with the numerical solution. Recently, Nithyadevi and Yang (2009) treats the case of a partially heated enclosure with Soret and Dufour coefficients around the density maximum. The effect of the various parameters (thermal Rayleigh number, center of the heating location, density inversion parameter, Buoyancy ratio number, Schmidt number, and Soret and Dufour coefficients) on the flow pattern and heat and mass transfer has been depicted. More recently, an extension of a compressible flow model to double-diffusive convection of binary mixtures of ideal gas enclosed in a cavity is presented by Sun *et al*. (2010).

The coupling of transient double diffusive convection with radiation is investigated numerically in a square cavity filled with a mixture of N_2 and CO_2 by Ibrahim and Lemonnier (2009). Their numerical results show that gas radiation modifies the structure of the velocity and thermal fields and accelerates the convergence to steady state in aiding case, while it favors the generation of instabilities and delays the arrival to a stable solution in opposing one. Their problem formulation is based on a low Mach number approximation. The authors analyzed the influence of density variation on transient solutions for pure thermal or pure solutal convection as well as for thermosolutal convection in the special case where the thermal and solutal buoyancy forces are equal in intensity either for aiding or for opposing cases.

Li *et al* (2010) studied the transition to chaos in double-diffusive Marangoni convection in a rectangular cavity with horizontal temperature and concentration gradients. They found that the supercritical solution branch takes a quasi-periodicity and phase locking route to chaos while the subcritical branch follows the Ruelle–Takens–Newhouse scenario.

A few of studies are interested in the 3D double diffusive natural convection. Bergeon and Knobloch (2002) studied bifurcations in the double diffusive convection in three dimensional cavity subjected to horizontal temperature and concentration gradients. They have proven that in certain conditions, the flow is unstable and the rate is periodic. In fact, the mechanism responsible for these oscillations is identified and the oscillations turned up to be an indirect consequence of the presence of a bifurcation to the longitudinal structures of the three dimensional flow which do not exists in a two dimensional formulation.

Sezai and Mohamad (2000) have demonstrated that, in case of a cube-shaped cavity, the structure of the flow of the thermosolutale natural convection, in the opposite case for values of buoyancy number superior to the unit, is purely three dimensional for certain values of the used parameters such as the buoyancy forces, the thermal Rayleigh and the Lewis numbers. They have noticed a variety of bifurcations and the formation of complex flow configurations.

More recently, the transient thermosolutal convection in a cubical enclosure having finite thickness walls filled with air, submitted to temperature and concentration gradients, is studied numerically by Kuznetsov *et al*. (2011). They analyzed the effect of Rayleigh number and the conductivity ratio on heat and mass transfer.

In the same way, the effect of the magnetic field on thermal convection within rectangular cavity has been studied by many authors. In fact, Oreper and Szekely (1983) have demonstrated that the presence of a magnetic field is an important factor determining the quality of the crystal. Ozoe and Okada (1989) investigated numerically three-dimensional buoyancy convection in a differentially heated cubical cavity with three different orientations of magnetic field along the axes. These authors have found that the magnetic field damps the flow most effectively when the magnetic field is imposed perpendicular to the heated vertical wall. It is the least effective when the magnetic field is horizontal and parallel to the heated vertical wall. Chamkha and Al-Naser (2002) studied the hydromagnetic double-diffusive convection in a rectangular enclosure with opposing temperature and concentration gradients.

They observed an oscillation in the flow in the absence of the magnetic field for a range of buoyancy ratio values. Also the heat and mass transfer mechanisms and the flow characteristics inside the enclosure depended strongly on the intensity of the magnetic field. In addition the effect of the magnetic field was found to reduce the heat transfer and fluid circulation within the enclosure.

When studying double-diffusive convection during alloyed semiconductor crystal growth in strong axial and transverse magnetic fields, Farrel and Ma (2004) mentioned that magnetic field must be

strong enough to eliminate flow oscillations but which moderately damped the melt motion in order to achieve both lateral and axial compositional uniformity in the crystal.

Sarris and al (2005) found that, in the presence of a magnetic field, the flow as well as the rate of heat and mass transfer is considerably affected. Borjini *et al* (2006) studied the effect of radiative heat transfer on the hydro-magnetic double-diffusive convection in two-dimensional rectangular enclosure for fixed Prandtl, Rayleigh, and Lewis numbers, Pr = 13.6, Ra = 10^5, Le = 2. Uniform temperatures and concentrations are imposed along the vertical walls while the horizontal walls are assumed to be adiabatic and impermeable to mass transfer. They proved that when progressively varying the optical thickness, multiple solutions are obtained which are steady or oscillatory accordingly to the initial conditions.

Double-diffusive convective flow in an inclined rectangular enclosure with heat generation is studied numerically by Mohamed A. Teamah *et al*. (2008) and (2012). In addition, a uniform magnetic field is applied in a horizontal direction. The numerical results are reported for the effect of thermal Rayleigh number, heat generation or absorption coefficient and the Hartmann number on the contours of streamline, temperature, and concentration as well as the dimensionless density.

Maatki *et al.* (2013) studied the effect of the magnetic field on the three dimensional double diffusive convection in cubic cavity filled with a binary mixture. In one hand, they found that when the flow is thermally dominated, the increasing of the intensity of the magnetic field causes a monotonic reduction of intensities of the main and three dimensional transverse flows. In the other hand, when the flow is solutally dominated an intensification of three dimensional flow with multi-cells structure of secondary flow is observed at Ha = 30.

The phenomenon of irreversibility expressed by the entropy generation is of great interest in the design of any thermodynamic system. The research works available on the analysis of entropy generation in double diffusive convection is still very low. Besides, the entropy generation in the double diffusion convection in enclosed cavities subjected to a magnetic field has not received much attention.

The generation of entropy in double-diffusive convection with an inclined cavity is numerically investigated by Magherbi *et al*. (2006). They showed that a moderate number of Lewis, the entropy generation increases with the Grashof number and the ratio of thermal buoyancy. The local irreversibility due to heat and mass transfer are almost identical and are located in the bottom heated and top cooled wall portions of the enclosure. The angle of inclination of the cavity has a significant effect on the entropy production for a thermal Grashof number equal to 10^4. In this case, the irreversibility increases to a maximum value for an angle equal to 45 °, then decreases and approaches the value of unity for the tilt angle of 180 °. Entropy generation of double-diffusive convection in the presence of rotation is studied by Sheng Chen (2011). They found that only fast rotation has significant influence on entropy generation distribution. Moreover, the share of irreversibility due to concentration diffusion increases quickly with N and it becomes the main contributor to entropy generation since N > 0.6. In another work, Sheng Chen and Rui (2011) studied the entropy generation of turbulent double-diffusive natural convection in a rectangle cavity. The authors examined the effects of thermal Rayleigh number, ratio of buoyancy forces and aspect ratio on entropy generation of turbulent double-diffusive natural convection. They concluded that the total entropy generation number increases with Ra, and the relative total entropy generation rates are nearly insensitive to Ra when Ra=10^9. They found also that the relative total entropy generation rate due to diffusive and thermal irreversibilities both are monotonic decreasing functions against aspect ratio while that due to viscous irreversibility is a monotonic increasing function with aspect ratio.

The influence of an oriented magnetic field on entropy generation in natural convection flow for air and liquid gallium is numerically studied by Eljery *et al*. (2010), they showed that transient entropy generation exhibits oscillatory behavior for air when a thermal Grashof number equal to 10^4 at small values of Hartmann number.

From the previous review, the problem of steady, laminar, hydromagnetic, entropy generation, double-diffusive natural convection flow inside a cubic enclosure was not explained. Because this situation is of fundamental interest and because it can have various possible applications such as crystal growth, geothermal reservoirs, nuclear fuel debris removal and solidification of metal alloys, it is of special interest to consider it in the present work. The top and bottom walls of the enclosure are assumed adiabatic and impermeable to mass transfer while the vertical walls are maintained at constant temperature and concentration. The magnetic Reynolds number is assumed small so that the induced magnetic field will be negligible. The originality of the present work is to highlight the influence of magnetic field on the three dimensional double diffusive convection as well as on the entropy generation in a cube-shaped cavity filled with a binary mixture (aqueous solution).

2. MATHEMATICAL FORMULATION AND NUMERICAL METHOD

Theconsidered system is presented in Fig. 1. A binary mixture (aqueous solution) is contained in a differentially heated cubic enclosure. Different concentrations are imposed at the left and right vertical walls, and no-heat and mass fluxes are imposed on the remaining walls with no slip boundary conditions for all velocity components. The direction of gravity is along the y-axis. An external magnetic field is applied within the X-direction. The fluid in this enclosure receives both

the buoyancy force resulting from heat and mass transfer through side walls and the Lorentz force resulting from the interaction between the fluid motion and the external magnetic field. The flow is assumed to be laminar and the binary fluid is considered Newtonian and incompressible. The physical properties of the fluid are supposed to be constant and the Boussinesq approximation is adopted. The Soret and Dufour effects are assumed to be negligible and the magnetic Reynolds number is considerably weak that the induced magnetic field is insignificant.

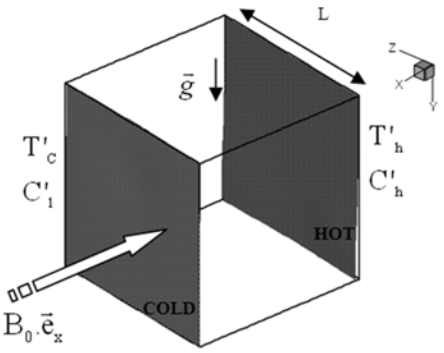

Fig. 1. Physical model and coordinated system.

The dimensionless variables used in this work are:

$$x=\frac{x'}{L};\ y=\frac{y'}{L};\ z=\frac{z'}{L};\ t=\frac{t'\alpha}{L^2};\ T=\frac{T'-T'_C}{T'_h-T'_C};$$

$$C=\frac{C'-C'_L}{C'_h-C'_L};\ (u_1,u_2,u_3)=\frac{(u'_1,u'_2,u'_3).L}{\alpha}$$

For numerical method we resorted to vorticity vector potential formalism in a three dimensional configuration (Ozoe and Okada al (1989)). The potential vector and the vorticity are defined respectively by:

$$\vec{\omega}=\vec{\nabla}\times\vec{u} \tag{1}$$

$$\vec{u}=\vec{\nabla}\times\vec{\psi} \tag{2}$$

The dimemsionless equations of conservation describing the transfer phenomena within the cavity are written in the form:

$$\vec{\nabla}^2\vec{\psi}=-\vec{\omega} \tag{3}$$

$$\frac{\partial\vec{\omega}}{\partial t}+(\vec{u}.\nabla)\vec{\omega}-(\vec{\omega}.\nabla)\vec{u}=\Pr\nabla^2\vec{\omega}+Ra.\Pr\left[\frac{\partial T}{\partial z},0,-\frac{\partial T}{\partial x}\right]-$$

$$Ra.\Pr.N\left[\frac{\partial C}{\partial z},0,-\frac{\partial C}{\partial x}\right]+\Pr.Ha^2.(\vec{\nabla}\times(\vec{j}\times\vec{e}_x)) \tag{4}$$

$$\frac{\partial T}{\partial t}+\vec{u}\vec{\nabla}T=\vec{\nabla}^2T \tag{5}$$

$$\frac{\partial C}{\partial t}+\vec{u}\vec{\nabla}C=\frac{1}{Le}\vec{\nabla}^2C \tag{6}$$

$$\vec{j}=-\vec{\nabla}\Phi+\vec{u}\times\vec{e}_x \tag{7}$$

$$\vec{\nabla}^2\Phi=\vec{\nabla}\left(\vec{u}\times\vec{B}\right)=-\vec{e}_x\vec{\omega} \tag{8}$$

Equations (3)-(8) represent respectively the balance laws of mass, linear momentum, thermal energy, concentration, Ohms laws and the balance laws of electric charge.

The dimensionless parameters figuring in these equations are:

$$Ha=B_0.L.\sqrt{\frac{\sigma_e}{\rho.\nu}},\ N=\frac{\beta_C(C_h-C_l)}{\beta_T(T_h-T_C)},$$

$$Ra=\frac{g.\beta_T(T_h-T_C).L^3}{\nu.\alpha},\ Pr=\frac{\nu}{\alpha},\ Le=\frac{\alpha}{D} \tag{9}$$

They represent respectively: Hartmann number, buoyancy ratio, Rayleigh number, Prandtl number and Lewis number.

The temperature and concentration boundaries conditions are given by:

$$T(0,y,z)=1,\quad C(0,y,z)=1,\quad T(1,y,z)=0,$$

$$C(1,y,z)=1,\ \frac{\partial T}{\partial n}=\frac{\partial C}{\partial n}=0 \text{ on other walls} \tag{10}$$

The boundaries conditions regarding vorticity and potential vector of velocity are:

For x=0 and x=1

$$\omega_1=0;\ \omega_2=-\frac{\partial u_3}{\partial x};\quad \omega_3=\frac{\partial u_2}{\partial x} \text{ and}$$

$$\frac{\partial\psi_1}{\partial x}=\psi_2=\psi_3=0 \tag{11-a}$$

For y=0 and y=1

$$\omega_1=\frac{\partial u_3}{\partial y};\quad \omega_2=0;\quad \omega_3=-\frac{\partial u_1}{\partial y} \text{ and}$$

$$\psi_1=\frac{\partial\psi_2}{\partial y}=\psi_3=0 \tag{11-b}$$

For z=0 and z=1

$$\omega_1=-\frac{\partial u_2}{\partial z};\quad \omega_2=-\frac{\partial u_1}{\partial z};\quad \omega_3=0 \text{ and}$$

$$\psi_1=\psi_2=\frac{\partial\psi_3}{\partial z}=0 \tag{11-c}$$

The boundaries conditions related to velocity, electric potential and current density on the inner surface are:

$$u_1=u_2=u_3=0;\ \frac{\partial\Phi}{\partial n}=0;\ \vec{j}.\vec{n}=0 \tag{12}$$

Thermal and diffusive gradient between the active walls of the cavity in addition to magnetic field effect causes entropy generation in the system. The local entropy generation in a three-dimensional flow is given by (Magherbi 2006):

$$S'_{gen}=\left\{\frac{k}{T_0^2}\left[\left(\frac{\partial T'}{\partial x'}\right)^2+\left(\frac{\partial T'}{\partial y'}\right)^2+\left(\frac{\partial T'}{\partial z'}\right)^2\right]\right\}$$
$$+\frac{\mu}{T_0}\left\{\begin{array}{l}2\left[\left(\frac{\partial u'_1}{\partial x'}\right)^2+\left(\frac{\partial u'_2}{\partial y'}\right)^2+\left(\frac{\partial u'_3}{\partial z'}\right)^2\right]\\+\left(\frac{\partial u'_2}{\partial x'}+\frac{\partial u'_1}{\partial y'}\right)^2+\left(\frac{\partial u'_3}{\partial y'}+\frac{\partial u'_2}{\partial z'}\right)^2+\left(\frac{\partial u'_1}{\partial z'}+\frac{\partial u'_3}{\partial x'}\right)^2\end{array}\right\}$$
$$+\left\{\begin{array}{l}\frac{R.D}{C_0}\left[\left(\frac{\partial C'}{\partial x'}\right)^2+\left(\frac{\partial C'}{\partial y'}\right)^2+\left(\frac{\partial C'}{\partial z'}\right)^2\right]\\+\frac{R.D}{T_0}\left[\left(\frac{\partial T'}{\partial x'}\right)\left(\frac{\partial C'}{\partial x'}\right)+\left(\frac{\partial T'}{\partial y'}\right)\left(\frac{\partial C'}{\partial y'}\right)+\left(\frac{\partial T'}{\partial z'}\right)\left(\frac{\partial C'}{\partial z'}\right)\right]\end{array}\right\}$$
$$+\frac{1}{T_0}.\frac{1}{\sigma_e}\left(J'^2_x+J'^2_y+J'^2_z\right) \qquad (13)$$

Where C_o and T_o are respectively the references concentration and temperature.

The dimensionless local entropy generation can be written as:

$$N_S=N_{S-th}+N_{S-fr}+N_{S-dif}+N_{S-th-dif}+N_{S-mag} \qquad (14)$$

Where:

$$N_{S-th}=\left[\left(\frac{\partial T}{\partial x}\right)^2+\left(\frac{\partial T}{\partial y}\right)^2+\left(\frac{\partial T}{\partial z}\right)^2\right] \qquad (15)$$

$$N_{S-fr}=\varphi_1\left\{\begin{array}{l}2\left[\left(\frac{\partial u_1}{\partial x}\right)^2+\left(\frac{\partial u_2}{\partial y}\right)^2+\left(\frac{\partial u_3}{\partial z}\right)^2\right]+\\\left[\left(\frac{\partial u_2}{\partial x}+\frac{\partial u_1}{\partial y}\right)^2+\left(\frac{\partial u_3}{\partial y}+\frac{\partial u_2}{\partial z}\right)^2+\left(\frac{\partial u_1}{\partial z}+\frac{\partial u_3}{\partial x}\right)^2\right]\end{array}\right\}$$

(16)

$$N_{S-dif}=\left[\left(\frac{\partial C}{\partial x}\right)^2+\left(\frac{\partial C}{\partial y}\right)^2+\left(\frac{\partial C}{\partial z}\right)^2\right] \qquad (17)$$

$$N_{S-th-dif}=\varphi_3\left[\left(\frac{\partial T}{\partial x}\right)\left(\frac{\partial C}{\partial x}\right)+\left(\frac{\partial T}{\partial y}\right)\left(\frac{\partial C}{\partial y}\right)+\left(\frac{\partial T}{\partial z}\right)\left(\frac{\partial C}{\partial z}\right)\right]$$

(18)

$$N_{S-mag}=\varphi_4.Ha^2\left(J_x^2+J_y^2+J_z^2\right)=\varphi_4.Ha^2.J^2 \qquad (19)$$

Where N_{S-th}, N_{S-fr}, N_{S-dif}, $N_{S-th-dif}$ and N_{S-mag} are respectively defined as local dimensionless entropy generation due to heat transfer, fluid friction, mass transfer by pure concentrations gradients, mass transfer by mixed product of concentration and thermal gradients and magnetic field.

φ_1, φ_2, φ_3 and φ_4 are irreversibility distribution ratios related to velocity gradients, concentrations gradients, mixed product of concentration and thermal gradients and magnetic field, respectively.

Dimensionless irreversibility distribution ratios (φ_1, φ_2, φ_3 and φ_4) are given by (Magherbi *et al.* (2006):

$$\varphi_1=\varphi_4=\frac{\mu.\alpha^2.T_0}{L^2.k.\Delta T'^2}; \qquad \varphi_2=\frac{R.D.T_0}{k.C_0}\left(\frac{\Delta C'}{\Delta T'}\right)^2;$$
$$\varphi_3=\frac{R.D}{k}\left(\frac{\Delta C'}{\Delta T'}\right) \qquad (20)$$

In the present work, the dimensionless irreversibility ratios are fixed respectively at $\varphi_1=\varphi_4=10^{-4}$, $\varphi_2=0.5$, $\varphi_3=10^{-2}$ (Magherbi *et al.* 2006).

Total dimensionless entropy generation is obtained by a numerical integration of dimensionless local entropy generation through the entire volume of the cavity:

$$S_{tot}=\int_v N_s.dv=\int_v\left(N_{S-th}+N_{S-fr}+N_{S-dif}+N_{S-th-dif}+N_{S-mag}\right)dv$$
$$S_{tot}=S_{th}+S_{fr}+S_{dif}+S_{th-dif}+S_{mag} \qquad (21)$$

The local Nusselt and Sherwood numbers, have the following expressions:

$$Nu=\left.\frac{\partial T}{\partial x}\right|_{x=0.1} \quad ; \quad Sh=\left.\frac{\partial C}{\partial x}\right|_{x=0.1} \qquad (22)$$

The Nusselt and Sherwood average numbers on the walls have the following expressions:

$$\overline{Nu}=\int_0^1\int_0^1 Nu.\partial y.\partial z \quad \overline{Sh}=\int_0^1\int_0^1 Sh.\partial y.\partial z \qquad (23)$$

The control volume finite method is used to discretize equations (1)-(8). The power law scheme for treating convective terms and the fully implicit procedure to discretize the temporal derivatives are retained. The grid is uniform in all directions with additional nodes on boundaries. The successive relaxation iterating scheme is used to solve the resulting non-linear algebraic equations. More information on the numerical method is in the work of Borjini *et al.* (2005).

The solution is considered acceptable when the following convergence criterion is satisfied for each step of time:

$$\sum_i^{1,2,3}\frac{\max\left|\psi_i^k-\psi_i^{k-1}\right|}{\max\left|\psi_i^k\right|}+\max\left|T^k-T^{k-1}\right|+\max\left|C^k-C^{k-1}\right|\le 10^{-5} \qquad (25)$$

3. GRID CONSIDERATION AND VALIDATION

The results presented in Table.1 show that the grid of (51x51x51) satisfies the grid independence. The time step is chosen to be 10^{-4}. The convergence criterion is to reduce the maximum mass residual of the grid control volume below 10^{-5}.

The numerical code is validated against the results of Sezai and Mohamed (2000), (Fig. 2). It is noted the concordance between the results.

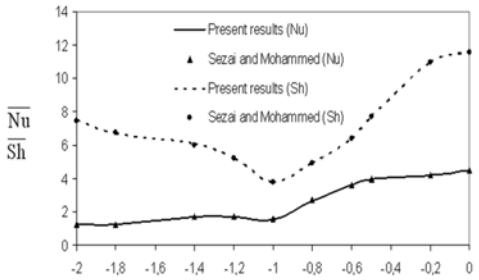

Fig. 2. Comparison between the present results and those of Sezai and Mohamed (2000)(Ra = 10^5, Pr=10 and Le=10).

The validation of the code has been done also by means of the Benchmark solution of the work of Chamkha and Al-Naser (2002)who studied the double diffusive convection in a rectangular cavity in the presence of a magnetic field for Ra = 10^5, Pr=1, Le = 2 and N = 1. Table 1 shows the values of the average Nusselt and Sherwood numbers obtained when the magnetic field is oriented toward x-direction, for different values of Ha. The difference, between the two results is less than 1.5%.All the values shown in this table are converted according to the dimensionless form of Chamkha and Al-Naser. (2002).

4. RESULTS AND DISCUSSION

4.1 Effect of Buoyancy Ratio on Flow Structure, Iso-Temperatures and Iso-Concentrations in Absence of Magnetic Field

Fig.3 shows some particles trajectories for different buoyancy ratio (N). When N=-0.5, the flow structure is characterized by one central vortex turning in the clockwise direction. The flow structure is thermally dominated. By increasing N, the intensity of the solutal volume forces increases. When N=-2, it is noted that the flow structure is characterized by one central vortex turning counter clockwise. Beside, two other vortex turning clockwise and situated on the top and bottom of the cavity. It is also noted that the flow structure is characterized by a spiraling form.

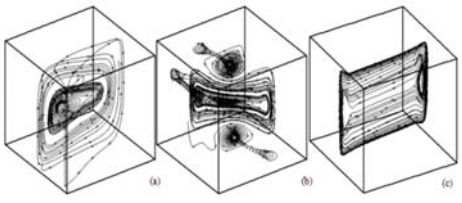

Fig. 3. Some particles trajectories (a: N=-0.5, b: N=-2 and c: N=-10).

The intensity of the thermal and solutal volume forces becomes competitive. In fact, the flow structure is composed by one solutal vortex situated in the core region of the cavity and two thermal vortex in the top and bottom of the cavity.

By increasing the buoyancy ratio to -10, the flow structure becomes solutal dominated and characterized by one vortex with two inner cells turning counter clockwise.

Fig.4 shows the effect of buoyancy ratio on the isothermals surfaces. For low value of buoyancy ratio (N=-0.5), the isothermals surfaces are stratified in vertical direction except near the insulated wall of the cavity and appear a horizontal surfaces in the core region of the cavity. In addition, the thermal gradient is high near the bottom of the hot wall and the top of the cold wall. The three dimensional aspect of the iso-temperature is observed also by the distortion in z direction. When N=-2, the flow structure is reversed and the iso-temperature becomes verticals and parallels. The thermal gradient, near the bottom of the hot wall and the top of the cold wall, decreases. The three dimensional aspect of the iso-temperatures is attenuated. When the flow structure is dominated by the solutal volume forces (N=-10), the isothermals surfaces becomes tilted and parallels. The thermal gradient becomes higher near the top of the hot wall and the bottom of the cold wall.

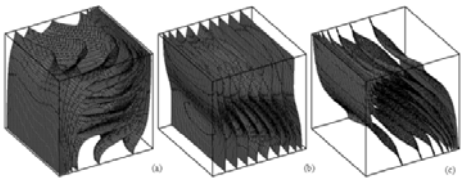

Fig. 4. Iso-temperatures for different buoyancy ratio (a: N=-0.5, b: N=-2 and c: N=-10).

Fig.5 illustrates the effect of buoyancy ratio on the iso-concentrations surfaces. For low value of buoyancy ratio (N=-0.5), as thermal buoyancy is much larger than solutal buoyancy, each the liquid in upper or lower layer penetrated into another layer along hot and cold wall, respectively. Consequently the liquid of low concentration exists near the top of the hot wall. The solutal gradient is high near the bottom of the high concentration wall and the top of the low concentration wall. The three dimensional aspect of the iso-cocentrations is also observed by the distortion in z direction. When N=-2, the flow structure is reversed and the iso-concentration becomes titled and parallels. The three dimensional aspect of the iso-concentrations is attenuated. For high value of buoyancy ratio (N=-10), solutal buoyancy becomes much larger than thermal buoyancy. The iso-concentrations surfaces are stratified in vertical direction and appear a horizontal surface in the core region of the enclosure. The solutal gradient becomes higher near the top of the high concentration wall and the bottom of the low concentration wall.

In the following, we will dedicate our work to study the effect of magnetic field on the flow structure and the generation of entropy in the case where the ratio of buoyancy is equal to -2.

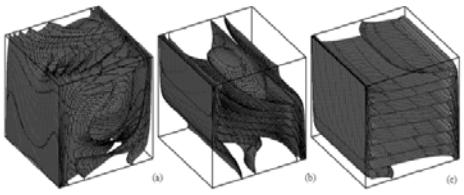

Fig. 5. Iso-concentrations for different buoyancy ratio (a: N=-0.5, b: N=-2 and c: N=-10).

4.2 Effect of Magnetic Field on Flow Structure, Isotemperatures and Iso-Concentrations

Fig 6-a demonstrates that the resulting flow structure is made up, of with two inner vortexes situated in the central region of the cavity, caused by solutal compositional forces, and two thermal vortexes, turning clockwise, situated in the upper and lower parts of the cavity. By applying a moderate magnetic field there is a disappearance of the thermal vortex situated in the bottom corner near the hot side. However, the intensification of the three-dimensional aspect is mainly observed on fig 6-e where the projection the velocity vector on the x=0.5 plan is characterized by the existence of eight symmetric secondary cells turning in opposite directions.

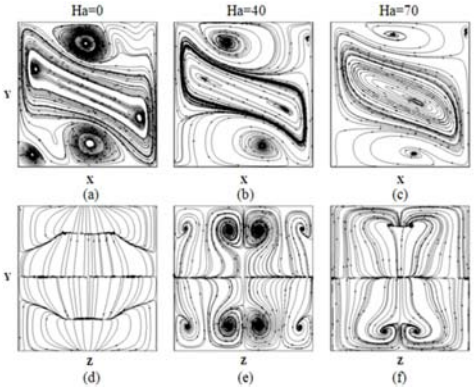

Fig. 6. Projection of flow lines on the mid X-Y plane (top), and the mid Y-Z plane (bottom) for Ra=10^5 and N= -2.

For higher Ha number values (Ha=70), (fig 6-c) the thermal vortexes become very small and the solutal vortex, occupies the central region of the cavity. In this case, the flow becomes conducted mainly by solutal volume forces. By analyzing fig 6-f, it is noted that the flow in the Z-direction is reduced. In fact, there is a disappearance of the secondary cells, thus a reduction in the three-dimensional aspect of the flow.

Fig.7 represents the iso-surfaces of concentration and of temperature for different Ha. By analyzing this figure, it is noted that for Ha=0, the iso-surfaces of temperature are transversally distorted in the central region of the cavity. The intensification of the magnetic field induces a decrease of these distortions (fig. 7-b) and and a reduction of the temperature gradient near the active walls. By further increasing Ha to 70, reduce the 3Deffect and iso-surfaces of temperature become quasi-vertical (fig 7-c). On fig. 7-a', a vertical stratification of concentration is noted. The solutal gradient is higher near the active walls. The increase of the Hartmann number (Ha=40) shows a decrease in the level of solutal gradient near the active sides and a remarkable transversal distortions (fig. 7-b'). For Ha =70, the 3d effects are reduced (fig. 7-c').

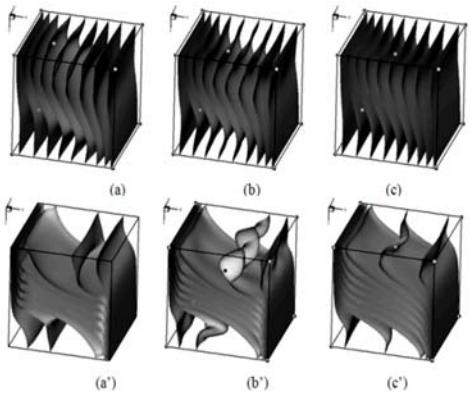

Fig. 7. Iso-surfaces of temperature (on the top) and concentration (on the bottom) for N=-2, (a,a') : Ha=0 ; (b,b') : Ha=40 and (c,c') Ha=70.

4.3 Effect of Hartmann Number (Ha) on the Local Nusselt and Sherwood Numbers

Figs. 8 and 9 are plotted to explore the effect of Hartmann number (Ha) on the distribution local Nusselt and Sherwood numbers over the hot wall. The following parameters are kept constant N=-2, Ra=10^5 and $0 \leq Ha \leq 70$. As shown in Fig. 8, the local Nusselt number has maximum values at the cavity top and its value decreases moving downwards. It is shown on Fig. 5-b that the temperature gradient is maximal at the cavity top and it decreases moving downwards reaching the minimum at the cavity bottom. This is noticed for all values of Hartmann number.

In addition, Fig. 8 shows that the local Nusselt number decreases as Hartmann number (Ha) increases. For the same position on the hot wall the local Nusselt number decreases as Ha increases. This occurs due to the magnetic damping effect that suppresses the overall heat transfer in the enclosure. Subsequently, the highest value for the local Nusselt number is at Ha =0 and the lowest value is at Ha=70.

Furthermore, Fig. 9 shows similar contributions for the effect of Hartmann number (Ha) on the local Sherwood number. The main difference is that the local Sherwood number generally has higher values than the local Nusselt number. Again, the highest value for the local Sherwood number is at Ha =0 and the lowest value is at Ha=70.

We observe also that the 3D aspect of the local Nusselt number and the local Sherwood number is more pronounced at the cavity bottom.

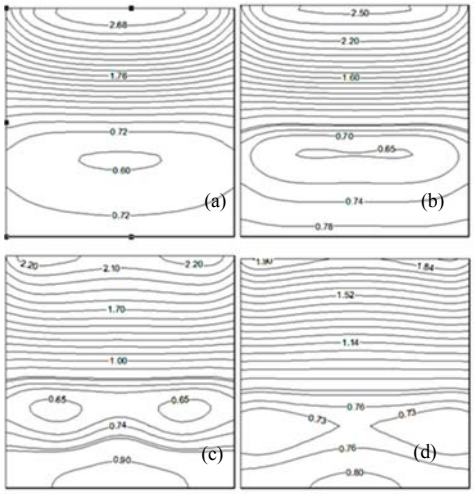

Fig. 8. The local Nusselt number for different Hartmann number (a: Ha=0, b: Ha=20, c: Ha=40 and d: Ha=70).

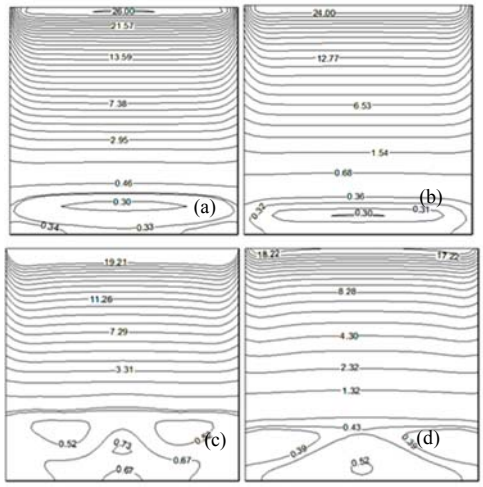

Fig. 9. The local Sherwood number for different Hartmann number (a: Ha=0, b: Ha=20, c: Ha=40 and d: Ha=70).

4.4 Effect of Hartmann Number (Ha) on the Average Nusselt and Sherwood Numbers

Fig. 10plots the effect of Hartmann on the average Nusselt and Sherwood numbers. The figure shows that the magnetic field effect is to suppress the heat and mass transfer within the cavity by decreasing the average Nusselt number and Sherwood numbers. This decrease is more pronounced for Sh. In fact, there is a declination of 30% compared to the case without magnetic field.

4.5 Effect of Magnetic Field on the Entropy Generation

Fig. 11 presents the local entropy generation due to the thermal gradient in case of solutal dominated regimes**.** For Ha=0 and 20, a region along the diagonal that connecting the top corner of the hot wall and the bottom corner of the cold wall shows high heat transfer irreversibility due to high temperature gradient in that region. In the other region of the cavity, the thermal entropy generation is negligible. By increasing Hartmann number to Ha=70, there is a decrease of the temperature gradient and of the magnitude of the local thermal entropy. The irreversibility contours become concentrated in the top corner of hot wall and in the bottom corner of the cold wall. The weak central entropy generation is linked to vertical compositional stratification.

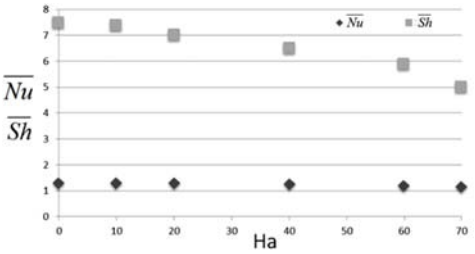

Fig. 10. Average Nusselt and Sherwood numbers according to Ha, for Ra=10^5 and N=-2.

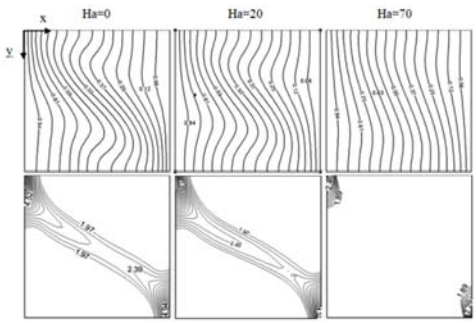

Fig. 11. Isotherm lines (top) and Local entropy generation due to thermal irreversibility N_{S-th} (bottom) on the X-Y plane for different Ha, Ra=10^5 and N = -2.

Fig. 12 shows that, for Ha= 0, the concentration gradient is higher near the top of highly concentrated wall and the bottom of poorly concentrated wall. Corresponding distribution on the local entropy generation due to mass transfer depicts that the entropy generation is higher in these regions. For Ha=20 and 70, some irreversibility is created far from the active walls due to increase of concentration gradient on z-directionin that region.

By analyzing fig.13, it is noted that the local entropy generation due to viscous effect occurs along the walls with the magnitudes of 11.69. The frictional irreversibility due to fluid flow is found to be lower compared to the case of thermal dominated flow. When Ha=20, a significant values of N_{S-fr} are found in the interior region of the cavity. By increasing Hartmann number, it is observed that the magnitude of the frictional irreversibility becomes low compared to the case of Ha=0.

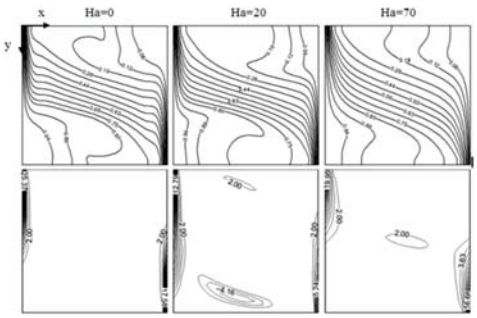

Fig. 12. Concentration lines (top) and local entropy generation due to concentration gradient irreversibility N_{S-dif} (bottom) on the X-Y plane for different Ha,Ra = 10^5 and N = -2.

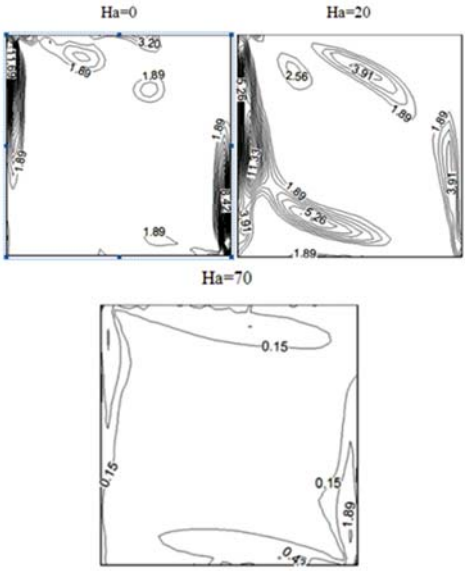

Fig. 13. Local entropy generation due to viscous effects irreversibility N_{S-fr} on the X-Y plane for different Ha, Ra = 10^5 and N = -2.

Fig.13-b presents the irreversibility due to the magnetic field. For Ha=20, the distribution of the local entropy generation due to magnetic field depicts that the entropy generation is higher at the upper portion of the hot wall and the down portion of the cold wall. The irreversibility due to magnetic field is also found to be produced in the core region of the cavity. For strongly damped flow, the local entropy generation due to magnetic field is higher near the cold wall than the hot one. In order to explain more this result, the fig.14-ais plotted, which shows the y-component of the Lorentz forces in the middle x-y plan. This force opposes the flow near the actives walls. For strongly damped flow, the magnitude of the Lorentz forces is the lowest near the cold wall. Therefore the attenuation of the flow velocity is lower near the cold wall compared to the hot wall. By consequence, the intensity of electric current density is higher near the cold wall compared to the hot one; which induces a great irreversibility in this region.

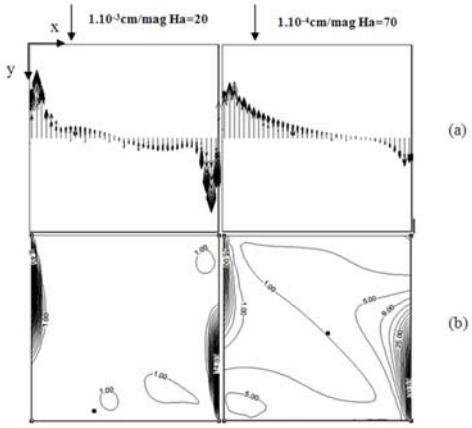

Fig. 14. Y-component of Lorentz forces (top) and Local entropy generation due to magnetic field irreversibility N_{S-mag} (bottom) on the X-Y plane for different Ha, Ra=10^5 and N = -2.

By analyzing the fig.15, it is found that, in absence of magnetic field, the total irreversibility is concentrated near the actives walls**.** It is situated by portion in the top of hot wall and in the bottom of cold wall. For Ha=20, there is an appearance of the total irreversibility in the core region. For higher Hartmann number, the irreversibility disappears in the core region and becomes concentrated near the active walls.

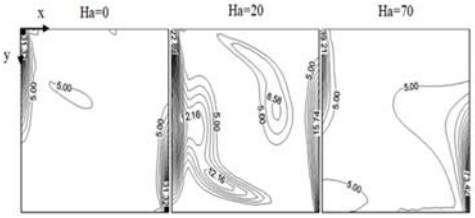

Fig. 15. Local entropy generation due to total irreversibility N_s on the X-Y plane for different Ha, Ra=10^5 and N = -2.

Fig.16 represents the variation of S_{fri}, S_{th}, S_{diff}, S_{mag} and S_{tot} according to Hartmann number in case of solutal dominated regime. It is clear that S_{fri}, S_{th} and S_{diff} decrease according to Ha. The entropy generation due to viscous effect decrease by 70% going from Ha=20 to Ha=70. The total entropy generation increases by 50% moving from a H= 0 to Ha =40. When the Hartmann number is greater than 30, the total entropy S_{tot} follows a polynomial equation:

$$S_{tot} = 0.0026\ Ha^2 - 0.19\ Ha + 8.9\ .$$

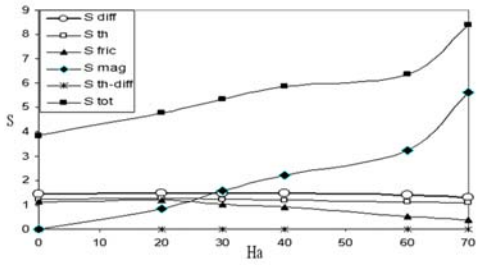

Fig. 16. Variation of entropy generation according to Ha, for Ra = 10^5 and N = -2.

5. CONCLUSION

In the present work, the three-dimensional mathematical model for natural double diffusive convection and entropy generation in a cubic enclosure under an external magnetic field was presented as well as the boundary conditions. The effect of magnetic field on entropy generation due to the thermo-solutal natural convection in a cubic enclosure was analyzed. Different behaviors of flow and entropy generation were observed when changing Ha. The main findings of the present investigation can be summarized as follows:

- The three-dimensional aspect of the flow structure depends on the intensity of the magnetic field. When Ha is greater than 40, a reduction of 3D flow structure is observed.
- The magnetic field reduces the heat transfer and fluid circulation within the enclosure due the retardation effect of the electromagnetic force.
- The three-dimensional aspect of the distribution of the local Nusselt number and the local Sherwood number is more pronounced at the cavity bottom.
- The local entropy generation is localized near the top of the hot wall with higher concentration and the bottom of the cold wall conversely to the case of thermal dominated.
- The total entropy generation manifests a monotonic increasing behavior with Hartmann number.
- Both thermal and solute horizontal stratifications cause weak balk entropy generation. However 3D concentration distribution, in presence of magnetic field, increases irreversibility in the core of the enclosure.

REFERENCES

Beghein, C., F. Haghighat and F. Allard (1992). Numerical study of double-diffusive natural convection in a square cavity. *International Journal of Heat and Mass Transfer (35), 833-846.*

Bergeon, A. and E. Knobloch (2002). Natural doubly diffusive convection in three-dimensional enclosures. *Physics of fluids (14), 3233–3250.*

Borjini, M. N., H. B. Aissia, K. Halouani and B. Zeghmati (2006). Effect of optical properties on oscillatory hydromagnetic double-diffusive convection within semitransparent fluid. *International Journal of Heat and Mass Transfer (49), 3984-3996.*

Borjini, M. N., K. Lioua, N. Daouas and H. B. Aissia (2005). Hydromagnetic double-diffusive laminar natural convection in a radiatively participating fluid. *Numer. Heat Transfer part A (48), 483-506.*

Chamkha A. J. and H. Al-Naser (2002). Hydromagnetic double-diffuse convection in a rectangular enclosure with opposing temperature and concentration gradients. *Int. J. Heat Mass Transfer (45), 2465-2483.*

Costa, V. A. F. (1997). Double-diffusive natural convection in a square enclosure with heat and mass diffusive walls. *International Journal of Heat and Mass Transfer (40), 4061-4071.*

ElJery, A. E., N. Hidouri, M. Magherbi and A. B. Brahim (2010). Effect of an external oriented magnetic field on entropy generation in natural convection. *Entropy (10),1391-417.*

Farrell, M. V. and N. Ma (2004). Macrosegregation during alloyed semiconductor crystal growth in strong axial and transverse magnetic fields. *Int. J. Heat Mass Transfer (47), 3047-3055.*

Gobin, D. and R. Bennacer (1996). Cooperating thermosolutal convection in enclosures II. Heat transfer and flow structure. *Int. J. Heat Mass Transfer (39), 2683-2697.*

Ibrahim, A. and D. Lemonnier (2009). Numerical study of coupled double-diffusive natural convection and radiation in a square cavity filled with A N_2–CO_2 mixture. *International Communications in Heat and Mass Transfer (36), 197-202.*

Kuznetsov, G. V. and M. A. Sheremet (2011). A numerical simulation of double-diffusive conjugate natural convection in an enclosure. *International Journal of Thermal Sciences 1878-1876.*

Li, Y., Z. W. Chen and J. M. Zhan (2010). Double-diffusive Marangoni convection in a rectangular cavity- Transition to chaos. *International Journal of Heat and Mass Transfer (53), 5223-5231.*

Maatki, C., L. Kolsi, H. F. Oztop, A. Chamkha, M. N. Borjini, H. Ben Aissia and K. Al-Salem (2013). Effects of magnetic field on 3D double diffusive convection in a cubic cavity filled with a binary mixture. *International Communications in Heat and Mass Transfer (46), 86-95.*

Magherbi, M., H. Abbassi, N. Hidouri and A. B. Brahim (2006). Second law analysis in convective heat and mass transfer. *Entropy, 1-*

17.

Makayssi, T., M. Lamsaadi, M. Naïmi, M. Hasnaoui, A. Raji and A. Bahlaou (2008). Natural double-diffusive convection in a shallow horizontal rectangular cavity uniformly heated and salted from the side and filled with non-Newtonian power-law fluids. *Energy Conversion and Management (49), 2016-2025*.

Mohamed, A. T (2008). Numerical simulation of double diffusive natural convection in rectangular enclosure in the presences of magnetic field and heat source. *International Journal of Thermal Sciences (47), 237-248.*

Mohamed, A. T., F. E. Ahmed and Z. M. Enass (2012). Numerical simulation of double-diffusive natural convective flow in an inclined rectangular enclosure in the presence of magnetic field and heat source. *International Journal of Thermal Sciences (52), 161-175*.

Nithyadevi, N. and R. Yang (2009). Double diffusive natural convection in a partially heated enclosure with Soret and Dufour effects*. International Journal of Heat and Fluid Flow (30), 902-910.*

Oreper, G. M. and J. Szekely (1983). The effect of an externally imposed magnetic field on buoyancy driven flow in a rectangular cavity. *J. Cryst. Growth (64), 505-515.*

Ozoe, H. and K. Okada (1989). The effect of the direction of the external magnetic field on the three-dimensional natural convection in a cubical enclosure*. Int. J. Heat Mass Transfer (32), 1939-1954.*

Sarris, I. E., S. C. Kakarantzas, A. P. Grecos and N. S. Vlachos (2005). MHD natural convection in a laterally and volumetrically heated square cavity. *International Journal of Heat and Mass Transfer (48), 3443-3453.*

Sezai, I. and A. A. Mohamad (2000). Double diffusive convection in a cubic enclosure with opposing temperature and concentration gradients. *Physics of Fluids (12), 2210-2223.*

Sheng, Ch. and R. Du (2011). Entropy generation of turbulent double-diffusive natural convection in a rectangle cavity. *Energy (36), 1721-1734.*

Sheng, C. (2011). Entropy generation of double-diffusive convection in the presence of rotation. *Applied Mathematics and Computation (217), 8575-8597*.

Sun, H., G. Lauriat, D. L. Sun and W. Q. Tao (2010). Transient double-diffusive convection in an enclosure with large density variations. *International Journal of Heat and Mass Transfer (53), 615-625.*

Trevisan, V. O. and A. Bejan (1992). Combined heat and mass transfer by natural convection in a vertical enclosure. *International Journal of Heat and Mass Transfer 104-112.*